nature COMMUNICATIONS

ARTICLE

https://doi.org/10.1038/s41467-022-29072-3 OPEN

Molecular basis for allosteric agonism and G protein subtype selectivity of galanin receptors

Jia Duan[1,2,13], Dan-Dan Shen[3,13], Tingting Zhao[4,5,13], Shimeng Guo[4,5,13], Xinheng He[1,2], Wanchao Yin[1], Peiyu Xu[1], Yujie Ji[1,2], Li-Nan Chen[3], Jinyu Liu[4,5], Huibing Zhang[3], Qiufeng Liu[1], Yi Shi[1], Xi Cheng[1], Hualiang Jiang[1,2,6], H. Eric Xu[1,2,6✉], Yan Zhang[3,7,8,9✉], Xin Xie[1,4,5,10,11✉] & Yi Jiang[1,6,12✉]

Peptide hormones and neuropeptides are complex signaling molecules that predominately function through G protein-coupled receptors (GPCRs). Two unanswered questions remaining in the field of peptide-GPCR signaling systems pertain to the basis for the diverse binding modes of peptide ligands and the specificity of G protein coupling. Here, we report the structures of a neuropeptide, galanin, bound to its receptors, GAL1R and GAL2R, in complex with their primary G protein subtypes G_i and G_q, respectively. The structures reveal a unique binding pose of galanin, which almost 'lays flat' on the top of the receptor transmembrane domain pocket in an α-helical conformation, and acts as an 'allosteric-like' agonist via a distinct signal transduction cascade. The structures also uncover the important features of intracellular loop 2 (ICL2) that mediate specific interactions with G_q, thus determining the selective coupling of G_q to GAL2R. ICL2 replacement in G_i-coupled GAL1R, μOR, 5-HT_{1A}R, and G_s-coupled β_2AR and D1R with that of GAL2R promotes G_q coupling of these receptors, highlighting the dominant roles of ICL2 in G_q selectivity. Together our results provide insights into peptide ligand recognition and allosteric activation of galanin receptors and uncover a general structural element for G_q coupling selectivity.

[1] CAS Key Laboratory of Receptor Research, Shanghai Institute of Materia Medica, Chinese Academy of Sciences, Shanghai 201203, China. [2] University of Chinese Academy of Sciences, Beijing 100049, China. [3] Department of Biophysics and Department of Pathology of Sir Run Run Shaw Hospital, Zhejiang University School of Medicine, Hangzhou, Zhejiang, China. [4] School of Chinese Materia Medica, Nanjing University of Chinese Medicine, Nanjing 210046, China. [5] CAS Key Laboratory of Receptor Research, National Center for Drug Screening, Shanghai Institute of Materia Medica, Chinese Academy of Sciences, Shanghai 201203, China. [6] School of Life Science and Technology, ShanghaiTech University, Shanghai 201210, China. [7] Liangzhu Laboratory, Zhejiang University Medical Center, Hangzhou, Zhejiang, China. [8] MOE Frontier Science Center for Brain Research and Brain-Machine Integration, Zhejiang University School of Medicine, Hangzhou, Zhejiang, China. [9] Key Laboratory of Immunity and Inflammatory Diseases of Zhejiang Province, Hangzhou, Zhejiang, China. [10] State Key Laboratory of Drug Research, Shanghai Institute of Materia Medica, Chinese Academy of Sciences, Shanghai 201203, China. [11] School of Pharmaceutical Science and Technology, Hangzhou Institute for Advanced Study, University of Chinese Academy of Sciences, Hangzhou 310024, China. [12] Lingang Laboratory, Shanghai 200031, China. [13] These authors contributed equally: Jia Duan, Dan-Dan Shen, Tingting Zhao, Shimeng Guo. ✉email: eric.xu@simm.ac.cn; zhang_yan@zju.edu.cn; xxie@simm.ac.cn; yijiang@simm.ac.cn

Neuropeptides are important signaling molecules in both the central and peripheral nervous system. At least 150 mature neuropeptides have been identified and most of them exert their biological functions via more than 100 G protein-coupled receptors (GPCR)[1]. The interactions of neuropeptides with cognate receptors and the downstream signaling are of great complexity[2], and are far from being fully elucidated.

Galanin, a 30-amino acid neuropeptide in humans, is widely distributed in the central and peripheral nervous systems and coexists with numerous classical neurotransmitters and neuropeptides. Galanin has been suggested to regulate metabolic homeostasis, reproduction, nociception, arousal/sleep, cognition, and stemness of cells[3]. Galanin exerts its action through three GPCRs, galanin receptor 1 (GAL1R), galanin receptor 2 (GAL2R), and galanin receptor 3 (GAL3R). The sequence homology among these receptors are 33.2% (GAL1R versus GAL3R), 35.5% (GAL1R versus GAL2R), and 53.8% (GAL2R versus GAL3R). These receptors are widely distributed in the central nervous system and show distinct but overlapping expression patterns[4]. Disruption of the galaninergic system is implicated in a large number of diseases, including chronic pain, mood disorders, epilepsy, and Alzheimer's disease, making galanin receptors attractive drug targets for the treatment of these diseases[3]. Considerable efforts have been devoted to developing synthetic galanin analogs displaying specific affinity towards galanin receptors; however, no active peptides have been approved so far.

Great progress has been made to clarify the molecular basis of galanin receptor recognition by galanin. The N-terminus of galanin (G^{1P}-V^{16P}, superscript refers to the amino acid position of galanin) is critical to receptor binding, with its C-terminal region showing minor importance[5–7]. G^{1P}, W^{2P}, N^{5P}, Y^{9P}, W^{10P}, and G^{12P} were then recognized as pharmacophores of galanin by alanine scanning analysis[5]. In addition, the importance of G^{1P} on recognition selectivity of galanin towards GAL1R over GAL2R and GAL3R was further identified[8]. At the galanin receptor side, mutagenesis analysis and molecular docking have identified several peptide-binding residues, thus revealing the possible underlying mechanisms of peptide recognition and selectivity at different galanin receptors[9–12]. However, these mechanisms remain poorly defined due to a lack of accurate structural information, which has hampered understanding the recognition mechanism of peptide and drug design targeting galanin receptors.

Specific GPCR couples with either a single or multiple G protein subtypes to transduce intracellular signals. The mechanism underlying the G protein-coupling selectivity remained one of the major issues in GPCR biology and has been proven to be complex[13–16]. It was thought that the coupling efficiency might depend on specific GPCR-G protein pair[16]. Although activated by the same peptide, GAL1R and GAL2R show selectivity for distinct G protein families. GAL1R couples with G_i protein, while GAL2R predominantly couples to $G_{q/11}$ protein and promiscuously activates $G_{i/o}$ and G_{12} pathways. However, the underlying mechanism of G protein preference for galanin receptors remain elusive.

Here, we report two cryo-EM structures of galanin-bound GAL1R and GAL2R in complex with G_i protein and G_q chimera, respectively. Combined with the functional analyses, these structures reveal a molecular mechanism of peptide recognition and receptor activation of galanin receptors. These structures also provide a template for understanding the critical role of ICL2 in the G_q-coupling efficiency of GAL2R and other G_s- and G_i-coupled class A GPCRs.

Results

Overall structures of galanin-bound GAL1R-G_i and GAL2R-G_q complexes. For the galanin-GAL1R-G_i complex, the full-length GAL1R, $G\alpha_i$ and $G\beta\gamma$ subunits, and scFv16 were co-expressed in *sf9* insect cells and then incubated with galanin for complex assembly. scFv16 was co-expressed to stabilize the GAL1R-G_i complex by binding to the interface between $G\alpha_i$ and $G\beta\gamma$ subunits of G_i heterotrimer[17]. For the galanin-GAL2R-G_q chimera complex, an additional NanoBiT tethering strategy was introduced to improve the stability of complex[18]. The C-terminus of truncated GAL2R (1-333) was connected to the LgBiT, while the HiBiT was fused to the C-terminus of the Gβ subunit. An engineered $G\alpha_q$ chimera was originated from the mini-$G\alpha_s$ scaffold with its N-terminus replaced by corresponding sequences of $G\alpha_{i1}$, providing an additional binding site for scFv16[19]. The equivalent engineered $G\alpha_q$ has been used for the structural determination of the G_q chimera-coupled ghrelin receptor and bradykinin receptor B2 complexes[20,21]. Thus, G_q refers to the engineered G_q chimera unless otherwise stated. GAL2R was co-expressed with $G\alpha_q$, $G\beta\gamma$ and then incubated with galanin in the presence of Nb35 to stabilize the receptor-G protein complex.

The two structures of galanin-bound GAL1R-G_i and GAL2R-G_q complexes were determined by single-particle cryo-electron microscopy (cryo-EM) at a global resolution of 2.7 and 2.6 Å, respectively (Fig. 1, Supplementary Table 1, Supplementary Fig. 1). The high resolution makes a sufficiently clear EM density for modeling all the components of two complexes. For the galanin-GAL1R-G_i complex, the final model contains GAL1R residues from positions 32 to 320. The majority of the residue side chains in the seven-transmembrane helical domains (TMDs), three extracellular loops (ECLs 1–3), and three intracellular loops (ICLs 1–3) of GAL1R were well-defined. In contrast to the receptor, only 16 amino acids (G^{1P}-V^{16P}) at the N-terminus of galanin can be clearly fitted (Supplementary Fig. 2). For the galanin-GAL2R-G_q complex, residues from 22 to 307 of GAL2R except for four residues ($D219^{5.70}$-$A222^{ICL3}$) in the TM5-ICL3 were also well-defined. Similar to galanin in the GAL1R-G_i complex, only the N-terminal portion of galanin (G^{1P}-P^{13P}) was well-defined in the galanin-GAL2R-G_q complex (Supplementary Fig. 2). The TMDs of both GAL1R and GAL2R are surrounded by annular detergent micelle mimicking the natural phospholipid bilayers (Fig. 1b, d). Within the micelle, five and two cholesterol molecules are clearly visible in the GAL1R and GAL2R EM density maps, respectively. These cholesterols are hydrophobically bound around the helix bundle of the receptor (Fig. 1c, e).

Unique binding mode of galanin at GAL1R and GAL2R. Structural comparison of the galanin-bound GAL1R and GAL2R with peptide GPCR complexes solved to date reveals a unique binding mode of galanin. Firstly, most of the N-terminal portion of galanin (L^{4P}-L^{11P}) in both galanin receptor complexes is organized in a canonical α-helix conformation with 3.6 residues each helical turn, followed by extended loops of peptide's C-terminus (Fig. 2a, b). This conformation is highly consistent with previously NMR models in a membrane-mimic environment. Galanin adopts a horseshoe-like shape in the NMR model, where its N-terminus folds as an α-helix, followed by a β-bend around P^{13P} and an uncertain conformation of the C-terminal region[22–24]. This N-terminal helical fold differs from the loop and β-strand conformation of other peptides bound to GPCRs, including DAMGO/μOR, ghrelin/GHSR, WKYMVm/FPR2, NTS_{8-13}/NTSR1, Ang II/AT1R, Ang II/AT2R, Des-Arg10-kallidin/B1R, bradykinin/B2R, CCK-8/CCK_AR, NMU/NMUR1, AVP/V2R, α-MSH/MC1R, and α-MSH/MC4R (Fig. 2c–o).

Furthermore, galanin exhibits a featured binding pose compared with other peptides bound to class A GPCRs solved so far. It is known that the majority of endogenous peptides insert into TMD binding cavity by their extreme N-terminus (DAMGO

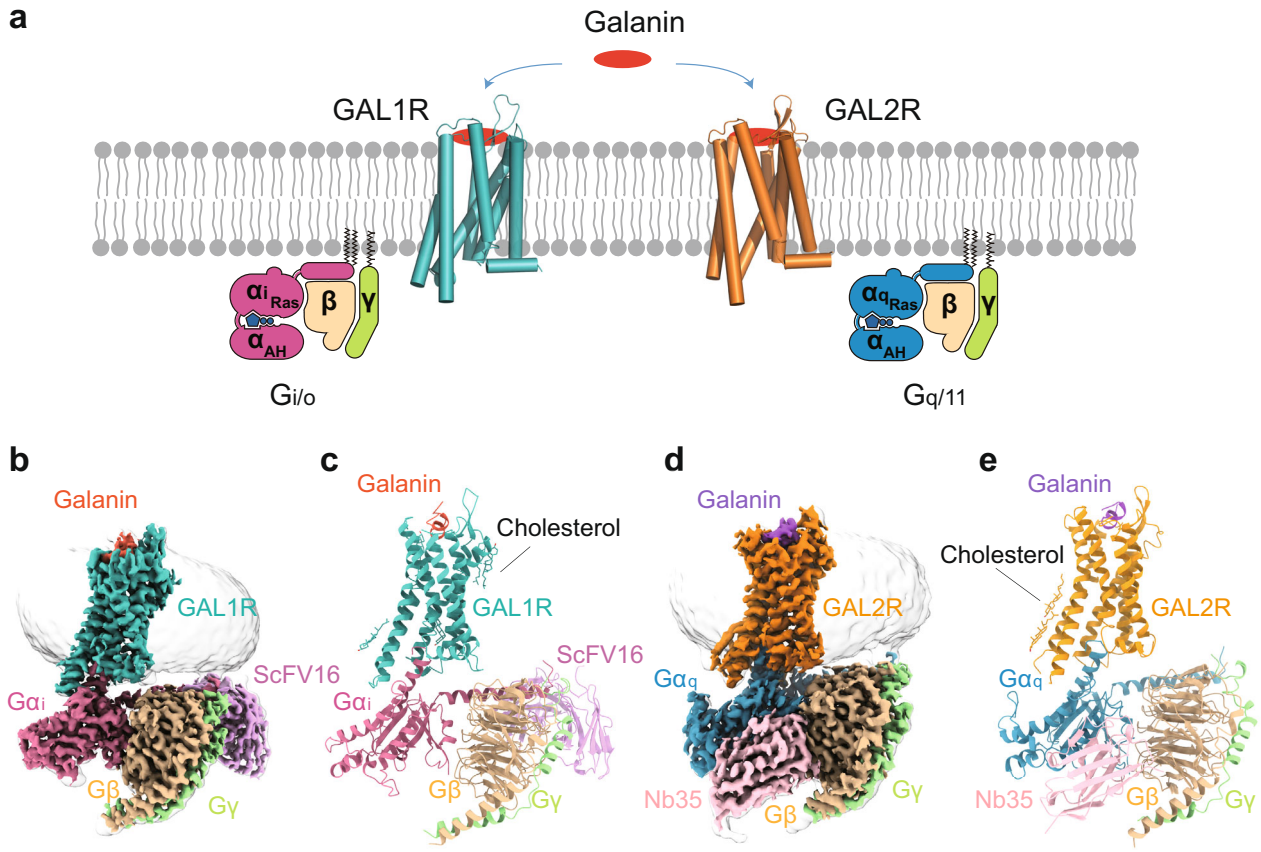

Fig. 1 Cryo-EM structures of galanin-GAL1R-G_i and galanin-GAL2R-G_q complexes. a Schematic illustration of G protein coupling of galanin receptors activated by galanin. Three-dimensional map (**b**) and the model (**c**) of the galanin-GAL1R-G_i complex. Three-dimensional map (**d**) and the model (**e**) of the galanin-GAL2R-G_q complex.

and ghrelin, Fig. 2c, d), C-terminus (WKYMVm, NTS_{8-13}, Ang II, des-Arg^{10}-kallidin, bradykinin, CCK-8, and NMU, Fig. 2e–l), or cyclic middle segment (AVP and α-MSH, Fig. 2m–o). Galanin was previously predicted to point to the helical cavity by its N-terminus[2]. Unexpectedly, galanin-GAL1R/GAL2R complex structures reveal a unique binding pose for galanin. It orients nearly horizontally to the cell membrane with a ~20° tilt, while Y^{9P} is the only amino acid inserted into the receptor helical cavity (Fig. 2a, b). As a result, the galanin-binding pocket dramatically differs in the topology compared with other structure-solved peptides for GPCRs. Intriguingly, although galanin itself binds in proximity to the extracellular surface of the receptor relative to other peptides, the pocket cavity of galanin receptors is as deep as that of other peptide GPCRs. Extra space exists in the galanin-binding pocket below the Y^{9P} (Fig. 2a, b). Designing galanin analogs or small molecular chemicals filling this empty region may offer a new therapeutic opportunity for galanin receptor-associated diseases. Together, these structures of galanin receptors present an unexpected binding pose of galanin and are added to the pool for enhancing the mechanistic understanding of class A GPCRs recognition by peptides.

Recognition mechanism of GAL1R and GAL2R by galanin. The well-resolved EM maps of the α-helical N-terminus of galanin and the receptor pocket enable accurate modeling and detailed interaction analysis between peptide and galanin receptors. Combined with functional analysis, these two complex structures reveal the recognition mechanism of galanin receptors by galanin. Globally, the N-terminus of galanin is located at the extracellular entrance of the TMD cavity and embraced by all three ECLs of both galanin receptors (Fig. 3a, b). Its N-terminus approaches TM2 and TM7, while the C-terminus points towards TM5 (Fig. 3b). Two conserved hydrophobic patches in galanin receptors interact with galanin, including ECL2 and a cluster comprising TM6, ECL3, and TM7 (Fig. 3c). Intriguingly, these two patches open a large extracellular crevice to accommodate bulky peptide helices and show more extensive hydrophobicity at the extracellular surface relative to the interior surface of the receptor helix core. This unique physiochemical feature leads to the hydrophobic N-terminal α-helix of galanin sandwiched by two hydrophobic patches and almost 'lay flat' at the extracellular face of galanin receptors, leaving Y^{9P} the only amino acid inserting into the helical core (Figs. 2a, b, and 3c). It is noted that the N-terminal of galanin (1-15) are conserved across different species (Supplementary Fig. 3a), indicating the conserved binding mode of galanin and the importance of this segment on peptide activity.

Specifically, three aromatic residues in ECL2 of GAL1R, including $F177^{ECL2}$, $F186^{ECL2}$, and $W188^{ECL2}$, constitute an extensive hydrophobic patch with L^{4P}, P^{13P}, and V^{16P} of galanin in the galanin-bound GAL1R complex (Fig. 3d, Supplementary Fig. 4a). In contrast, L^{4P} contacts with equivalent ECL2 residues with weaker hydrophobicity ($L169^{ECL2}$, $A170^{ECL2}$, and $L172^{ECL2}$) in GAL2R (Fig. 3e, Supplementary Fig. 4b). The structural observation is coincident with our peptide truncation assay. The C-terminal truncation of galanin to V^{16P} retained the binding and receptor activation potency of the full-length galanin. Further truncating galanin to P^{13P} did not affect its binding and receptor activation capacity for GAL2R but notably decreased its binding and activity for GAL1R (Supplementary Fig. 5b–e, Supplementary

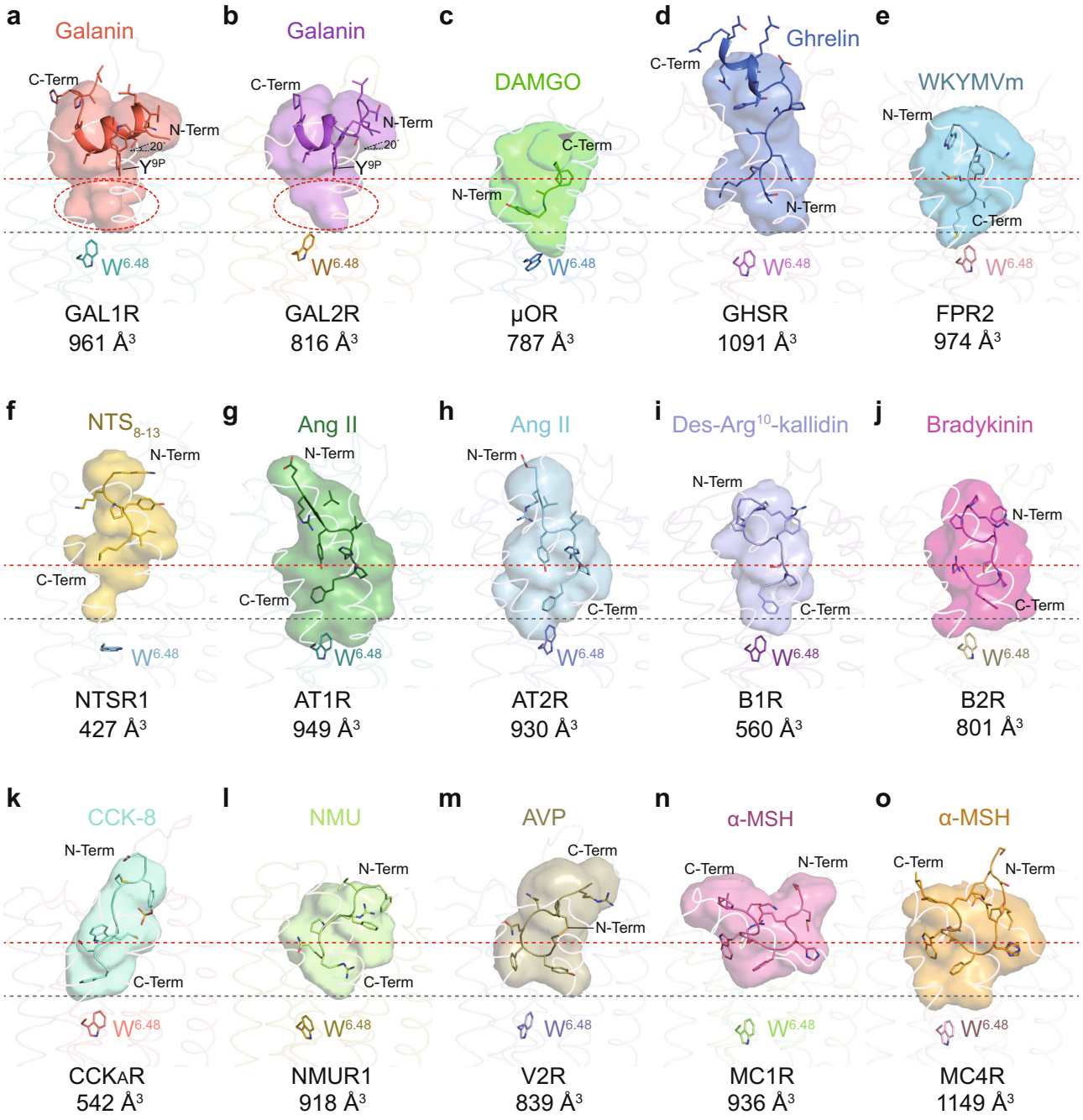

Fig. 2 Unique binding mode of galanin at GAL1R and GAL2R. a–o The binding modes of peptides at different peptide GPCRs. The peptides are shown in cartoon presentation and colored as indicated. The peptide-binding pockets are displayed as transparent surfaces with the same colors of specific peptides. The volume of each orthosteric pocket was measured by POVME 2.0[49]. The N-terminus (N-Term), C-terminus (C-Term) of peptides and volumes of peptide-binding pockets are indicated. The depths of galanin-binding and the pocket in galanin receptors are highlighted as dashed reference lines in red and black, respectively. **a** Galanin in GAL1R; **b** galanin in GAL2R; Tilt angles (20°) compared to cell membrane and Y^{9P} of galanin are indicated. Extra binding pockets beneath galanin are highlighted as red dashed ovals. **c** DAMGO in mu-opioid receptor (μOR, PDB: 6DDE); **d** Ghrelin in ghrelin receptor (GHSR, PDB: 7F9Y); **e** WKYMVm in formyl peptide receptor 2 (FPR2, PDB: 6OMM); **f** Neurotensin 8-13 (NTS_{8-13}) in neurotensin receptor 1 (NTSR1, PDB: 6OS9); Angiotensin II (Ang II) in angiotensin II receptor type 1 (AT1R, PDB: 6OS0, **g**) and type II (AT2R, PDB: 6JOD, **h**); **i** Des-Arg10-kallidin in bradykinin B1 receptor (B1R, PDB: 7EIB); **j** Bradykinin in bradykinin B2 receptor (B2R, PDB: 7F2O); **k** CCK-8 in cholecystokinin A receptor (CCK_AR, PDB: 7EZM); **l** Neuromedin U (NMU) in neuromedin U receptor 1 (NMUR1, PDB: 7VG6); **m** Arginine vasopressin (AVP) in vasopressin receptor 2 (V2R, PDB: 7DW9); **n**, **o** α-melanocyte-stimulating hormone (α-MSH) in melanocortin 1 receptor (MC1R, PDB: 7F4D, **n**) and melanocortin 4 receptor (MC4R, PDB: 7F53, **o**).

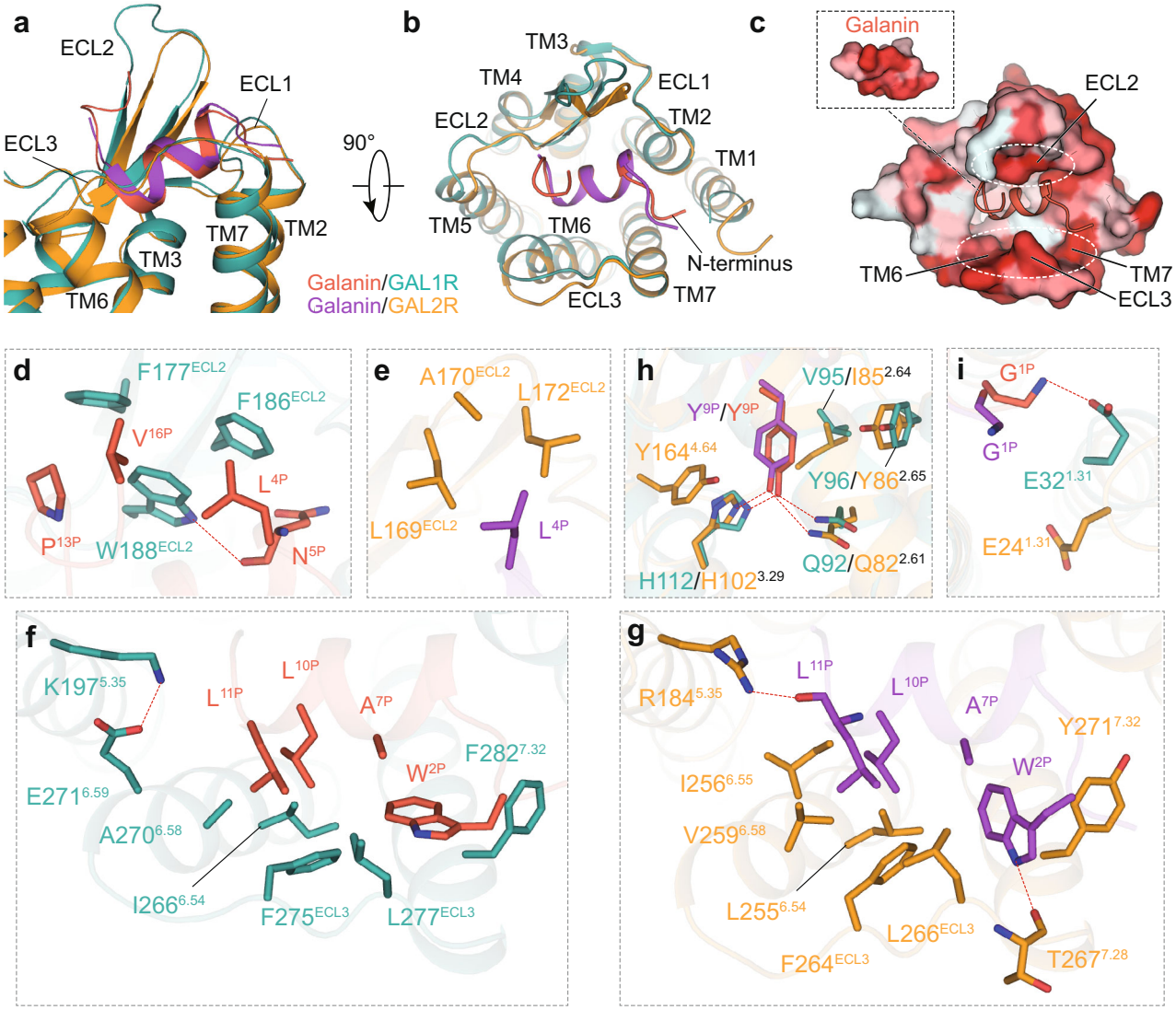

Fig. 3 Recognition mechanism of GAL1R and GAL2R by galanin. The overall binding pose of galanin in GAL1R and GAL2R in the side view (**a**) and extracellular view (**b**). **c** Two hydrophobic patches at the extracellular surface of the GAL1R binding pocket sandwich with galanin. Two hydrophobic patches are highlighted as white dashed ovals. Receptor surface is colored by hydrophobicity, from white for hydrophilic to red for hydrophobic. Detailed interactions between galanin and the hydrophobic patch in ECL2 of GAL1R (**d**) and GAL2R (**e**). The H-bond is shown as a red dashed line. Detailed interactions between galanin and the hydrophobic patch in TM6-ECL3-TM7 of GAL1R (**f**) and GAL2R (**g**). **h** Interactions between Y^{9P} and residues of two galanin receptors. **i** Detailed interactions between G^{1P} of galanin and two galanin receptors.

Table 2), which is consistent with the previous finding that GALP (1–60), which shares only 13 identical amino acids (9-21) with N-terminus of galanin (Supplementary Fig. 3b), displays a higher affinity for GAL2R over GAL1R[25,26]. In addition, the extensive hydrophobic interactions between ECL2 of GAL1R and galanin may explain the three additional amino acids EM densities of H^{14P}-A^{15P}-V^{16P} in the galanin-GAL1R-G_i complex (Supplementary Figs. 2 and 4). Alanine mutations of $F186^{ECL2}$ and $W188^{ECL2}$ in GAL1R but not the residues ($L169^{ECL2}$, $A170^{ECL2}$, and $L172^{ECL2}$) in ECL2 of GAL2R almost abolished the binding of galanin, indicating that the hydrophobic patch in ECL2 makes a greater contribution to galanin activity for GAL1R over GAL2R (Supplementary Figs. 6 and 7, Supplementary Tables 3 and 4). In addition, $W188^{ECL2}$ of GAL1R creates an additional H-bond with the backbone CO group of N^{5P}, while the corresponding polar interaction is absent between peptide and GAL2R (Fig. 3d, e).

In both galanin-bound receptor subtypes, W^{2P}, A^{7P}, L^{10P}, and L^{11P} of galanin face a similar hydrophobic patch comprised by TM6 ($I266/L255^{6.54}$ and $A270/V259^{6.58}$ for GAL1R/GAL2R), ECL3 ($F275/F264^{ECL3}$ and $L277/L266^{ECL3}$), and TM7 ($F282/Y271^{7.32}$). In addition, $I256^{6.55}$ of GAL2R are also involved in these hydrophobic interactions (Fig. 3f, g, Supplementary Figs. 7 and 8). These structural observations are consistent with the fact that substituting hydrophobic residues at ECL3 and 7.32 with alanine results in dramatically decreased binding and activation potency of galanin against two galanin receptors (Supplementary Figs. 6–8, Supplementary Tables 3 and 4). Regarding the binding motif on TM6, residues at 6.54 and 6.58 appear to show a greater impact on GAL2R compared with GAL1R. Besides hydrophobic interactions, W^{2P} of GAL2R forms an additional H-bond with the main chain CO group of $T267^{7.28}$ due to its rotameric state by ~90° relative to GAL1R (Fig. 3f, g). In addition, $K197^{5.35}$ of GAL1R forms an intramolecular salt bridge with $E271^{6.59}$, mutation of K197 does not affect ligand binding and receptor function, while the corresponding polar residue $R184^{5.35}$ of GAL2R interacts with the main chain CO group of L^{11P} (Fig. 3f, g), and contribute

significantly towards ligand binding and receptor function (Supplementary Figs. 6–8, Supplementary Tables 3 and 4).

As the only residue inserted into the receptor TMD cavity, Y^{9P} forms polar interactions with $Q^{2.61}$ and $H^{3.29}$, two conserved residues across GAL1R and GAL2R. Y^{9P} is also involved in hydrophobic interactions with V95/$I85^{2.64}$ and Y96/$Y86^{2.65}$ (GAL1R/GAL2R). Y^{9P} makes an additional hydrophobic interaction with $Y164^{4.64}$ of GAL2R relative to $Q174^{4.64}$ of GAL1R (Fig. 3h). It should be noted that Y^{9P} may make different contributions to galanin binding for two galanin receptor subtypes. Y^{9P}A substitution abolished the GAL2R binding by galanin, presenting a more significant effect relative to GAL1R (Supplementary Fig. 5b, c, Supplementary Table 2). In contrast to most of the Y^{9P}-interacting residues, which showed similar impaired effects on both galanin receptors, $H112^{3.29}$ does not affect the binding and activation activity of GAL1R. However, its equivalent residue $H102^{3.29}$ led to an abolished peptide binding and GAL2R activation (Supplementary Figs. 6–8, Supplementary Tables 3 and 4).

Furthermore, these two structures of galanin receptor complexes provide a template for understanding the receptor subtype selectivity of galanin analogs. Compared with the wild-type galanin, the G^{1P}-truncated galanin (2–16) exhibited a dramatically decreased binding activity to GAL1R but did not affect its activity to GAL2R, thus presenting a specificity for GAL2R (Supplementary Fig. 5b, c, Supplementary Table 2). Our structural observation supports this binding selectivity that the main chain NH group of G^{1P} forms an H-bond with $E32^{1.31}$ in GAL1R. Mutating $E32^{1.31}$ to arginine dramatically hampered GAL1R activation (Supplementary Fig. 8a, Supplementary Table 3). Conversely, G^{1P} does not form meaningful interactions with GAL2R and is discardable in GAL2R binding and activation (Fig. 3i, Supplementary Fig. 5c). This structural distinction also provides a rationale for the low selectivity of galanin segment 2-11 (ARM1896) for GAL1R and offers a template for designing "non-GAL1R" selective ligands[8]. Taken together, despite the similar binding mode of galanin peptide with GAL1R and GAL2R, galanin peptide shows a distinct interaction network towards GAL1R and GAL2R. Together, these findings may serve as a paradigm for understanding the galanin-binding mechanism and designing selective agonists towards galanin receptors.

The structural models of galanin receptors also offer potential insights into the recognition of other galanin-like peptides. Interestingly, a middle region (amino acids 9–21) of galanin-related peptide (GALP), a galanin homologue with biological activities to galanin receptors, are entirely identical to the first 13 amino acids of galanin (Supplementary Fig. 3b). This sequence feature logically supports the 'lay flat' binding pose of this peptide segment, which prevents the N-terminus of GALP from entering the binding cavity of galanin receptors. Mature spexin is a 14-amino acid peptide originating from a common ancestral lineage and shares conserved five of 14 amino acids with galanin, including Y^{9P} (Supplementary Fig. 3b). It exhibits cross-reactivity to galanin receptors, showing a high affinity for GALR2 but not GALR1 (Supplementary Fig. 9a)[27]. The first amino acid of spexin is different from galanin (Supplementary Fig 3b). Spexin did not activate GAL1R, further confirming the importance of the G^{1P} of galanin in activation of GAL1R, since G^{1P}-truncated galanin (2–16) showed dramatically reduced binding and activation of GAL1R but not GAL2R. Compared with galanin, spexin showed a similar overall activation pattern on GAL2R, with most of the receptor mutants showing consistent changes of both peptides' activities (Supplementary Figs. 8b and 9b, Supplementary Tables 4 and 5). Representatively, alanine mutation of residues surrounding Y^{9P} of galanin, including $Q82^{2.61}$, $I85^{2.64}$, $Y86^{2.65}$, $H102^{3.29}$, and $Y164^{4.64}$, dramatically hampered the activity of spexin (Supplementary Fig. 9b). This finding indicates that Y^{9P} from both peptides are probably located in a similar residue environment in GAL2R. Interestingly, substituting residues in ECL2, including $A170^{ECL2}$ and $L172^{ECL2}$, with alanine presented a more pronounced effect on spexin-induced GAL2R activation compared with galanin, indicative of a greater contribution of ECL2 on spexin activity (Supplementary Figs. 8b and 9b).

An unconventional activation mechanism of GAL1R and GAL2R. A structural comparison of GAL1R and GAL2R complexes to the inactive μOR (PDB: 4DKL), which shows sequence similarity to galanin receptors, offers a rationale for understanding the activation mechanism of galanin receptors. Compared with the inactive μOR, both GAL1R and GAL2R adopt fully active conformations, showing a pronounced outward displacement of the cytoplasmic end of TM6, a hallmark of class A GPCR activation, alongside with an inward movement of TM7 cytoplasmic end (Fig. 4a)[28].

Most of peptidic ligands, except for WKYMVm and Ang II (AT2R bound), showed a notable larger vertical distance to the highly conserved toggle switch $W^{6.48}$ (Fig. 2). Intriguingly, compared with other peptides, galanin is almost suspending on top of the helical cavity, holding only by two hydrophobic sidewalls, presenting a unique binding pose. Comprehensive alanine scanning mutagenesis and amino acid substitution analyses support that pocket residue, including those in two extracellular hydrophobic patches and helix bundle surrounding Y^{9P}, substantially contribute to receptor activation by disturbing galanin binding (Supplementary Figs. 6–8, Supplementary Tables 3 and 4). Hence, galanin is anticipated to function as an 'allosteric-like' peptide and remotely activates galanin receptors via an unconventional signaling transmission mechanism from the binding site to the cytoplasmic surface of GPCRs.

Intriguingly, several positively charged residues were seen between TM6 and TM7, including H263/$H252^{6.51}$, R285/$R274^{7.35}$, and H289/$H278^{7.39}$ (GAL1R/GAL2R) in both galanin receptors, which is less conserved in other class A peptide GPCRs (Fig. 4b, c). These residues are located below the galanin-binding site and may serve as a junctor to connect the peptide pocket to the toggle switch $W^{6.48}$ (Fig. 4b). Indeed, the alanine mutations of these residues caused significantly decreased galanin activities for both galanin receptors (Fig. 4d, e). Interestingly, different from other positively charged residues in both galanin receptors, $H252^{6.51}$ of GAL2R substantially contributes to the binding of galanin (Supplementary Figs. 6 and 7). Considering the absence of direct contact with galanin, $H252^{6.51}$ may trigger a distinct conformational change of GAL2R relative to GAL1R to disfavor the peptide binding. These results highlight the importance of these positively charged residues in propagating galanin agonism signals. This agonism signals may cause conformational changes of highly conserved "micro-switches", including toggle switch (Fig. 4f), PIF (Fig. 4g), DRY (Fig. 4h), and NPxxY (Fig. 4i), eventually lead to intracellular active-like conformational changes of galanin receptors.

The G protein interfaces of GAL1R and GAL2R. Structural superposition of GAL1R-G_i and GAL2R-G_q complexes by receptor reveals almost identical receptor conformations, with a root-mean-square deviation (R.M.S.D.) of 0.8 Å (Fig. 5a). However, the structural comparison of the two complexes reveals a difference in G proteins. The $Gα_i$ α5 helix of GAL1R-G_i complex shifts half-helical turn away from the helical cavity compared with that of the $Gα_q$ of GAL2R-G_q complex. Meanwhile, the $Gα_i$

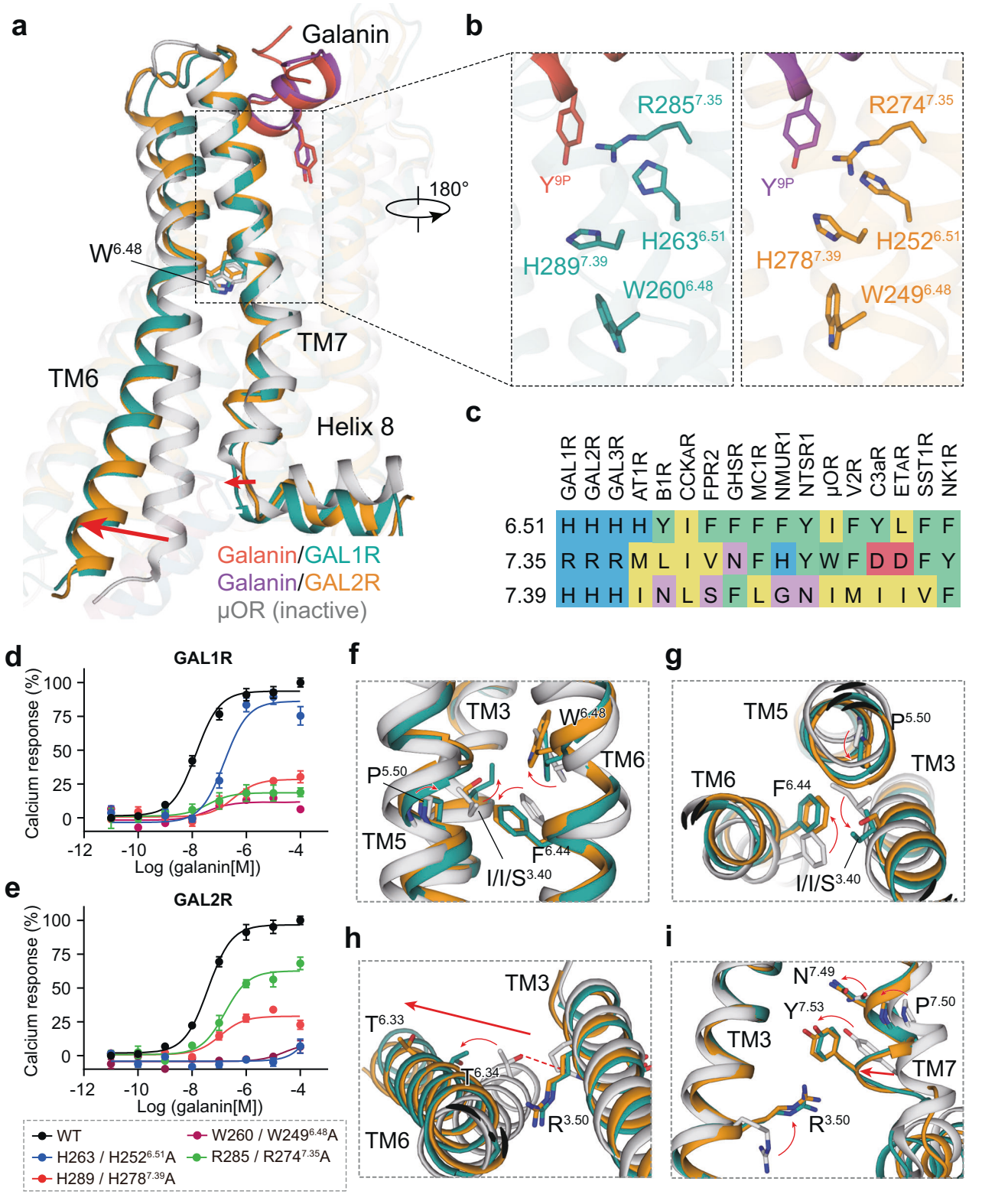

Fig. 4 The unconventional activation mechanism of GAL1R and GAL2R. a Structural comparison of GAL1R-G_i and GAL2R-G_q complexes with μOR in the inactive state (PDB: 6DKL). The outward movement of TM6 and inward shift of TM7 in galanin receptors relative to μOR are shown as red arrows, indicative of the fully active conformation of both galanin receptors. **b** Three positively charged residues involved in agonism signaling transmission of galanin in GAL1R (left panel) and GAL2R (right panel). **c** Sequence alignment of residues at 6.51, 7.35, and 7.39 in class A peptide GPCRs. The effects of mutation of three positively charged residues on galanin-induced activation of GAL1R (**d**) and GAL2R (**e**). WT and receptor mutants were transfected into HEK293/$G\alpha_{16}$ cells and intracellular calcium response was measured to reflect the activity of galanin. Data shown are mean ± S.E.M. of six independent experiments ($n = 6$). Source data are provided as a Source Data file. **f**–**i** The conformational rearrangement of residues in conserved "micro-switches" upon galanin receptors activation. In contrast to μOR in the inactive state, the conformational changes of "micro-switches" residues in toggle switch (**f**), PIF (**g**), DRY (**h**), and NPxxY (**i**) of GAL1R and GAL2R are indicated as red arrows. The movement of TM6 and TM7 are highlighted as red arrows.

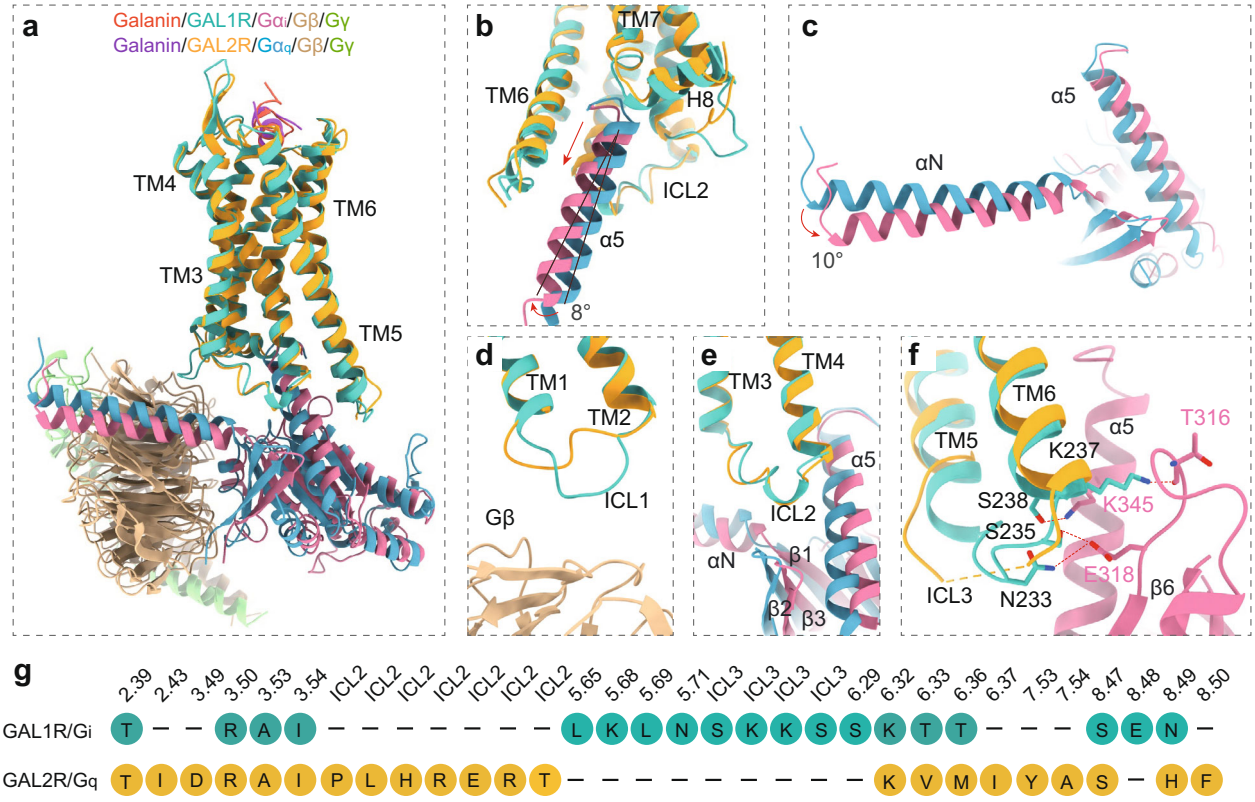

Fig. 5 The G protein interfaces of GAL1R and GAL2R. a Structural superposition of the GAL1R-G_i and GAL2R-G_q complexes. **b** Conformational comparison of α5 helix in GAL1R-G_i and GAL2R-G_q complexes. Compared to that of the GAL2R-G_q complex, the movement away from the receptor TMD cavity and an 8° shift of $G\alpha_i$ α5 helix of the GAL1R-G_i complex are indicated in red arrows. **c** Conformational comparison of αN helix of $G\alpha_i$ and $G\alpha_q$ subunits in both galanin receptor complexes. The αN of the $G\alpha_i$ subunit in the GAL1R-G_i complex shows a 10° rotation relative to the $G\alpha_q$ subunit in the GAL2R-G_q complex. Structural comparison between the $G\alpha_i$ and $G\alpha_q$ subunits and ICLs of both galanin receptors, including ICL1 (**d**), ICL2 (**e**), and ICL3 (**f**). **g** The profile of the G protein-coupling residues in GAL1R and GAL2R.

α5 helix of GAL1R-G_i complex shows an 8° shift towards TM6 (Fig. 5b), which translates into a 10° movement of the αN helix away from the cell membrane relative to the $G\alpha_q$ of GAL2R-G_q complex (Fig. 5c).

The overall assembly of GAL1R with G_i protein and GAL2R with G_q protein is similar to other class A GPCRs solved so far. The distal end of the α5 helix of the Gα subunit inserts into the cytoplasmic cavity of the receptor TMD, interacting with residues from the receptor TM4, TM5, TM6, ICL3, and helix 8, constituting a primary coupling interface between galanin receptors and G proteins (Supplementary Fig. 10). For the interfaces between ICLs of receptor and G protein, ICL1 of GAL1R shifts closer towards the Gβ subunit relative to GAL2R-G_q complex, introducing an additional interaction interface between ICL1 of the receptor and Gβ of G_i protein (Fig. 5d). ICL2 of both galanin receptors adopts a similar α-helical conformation and forms a conserved interface with residues at the αN/β1 hinge, β2/β3 loop, and α5 helix of the Gα subunit (Fig. 5e). In addition, compared with the G_q-coupled GAL2R complex, ICL3 of GAL1R shows a continuous density, which has not been mostly observed in G_i-coupled class A GPCRs, and forms extensive polar interactions with residues in α5 helix and α4/β6 loop of the $G\alpha_i$ subunit (Fig. 5f, g).

Of note, ICL2 of two galanin receptors displays distinct G protein-coupling features for two galanin receptors (Fig. 5g). Sequence analysis of ICL2 between both galanin receptors and representative class A GPCRs reveals that the conserved hydrophobic residue in ICL2 at 34.51, which often packs ICL2 against the conserved hydrophobic pocket in Gα subunit, is absent in GAL1R (Fig. 6a, b, d–h). Substituting R141$^{34.51}$ with hydrophobic leucine did not increase the activity of galanin, indicating a negligible contribution of this position to GAL1R-G_i coupling (Fig. 6i), which is consistent with the contention that the bulky hydrophobic residue at 34.51 may not be critical for primary GPCR-$G_{i/o}$ coupling[16]. It should be noted that the absence of hydrophobic residue at 34.51 is also observed in members of the chemokine receptor subfamily, including C-C chemokine receptor type 6 (CCR6, PDB: 6WWZ)[29]. However, the residue at 34.54 in ICL2 of CCR6 other than 34.51 participates in its interaction with the $G\alpha_i$ subunit (Fig. 6c, g). Differently, no substantial interactions were observed between ICL2 of GAL1R and the $G\alpha_i$ subunit. Different from ICL2 of GAL1R, L131$^{34.51}$ in ICL2 of GAL2R hydrophobically interacts with residues in the αN-α5 cleft of the $G\alpha_q$ subunit, constituting the other receptor-$G\alpha_q$ interface (Fig. 6d). This hydrophobic contact is critical to GAL2R-G_q protein coupling, which is supported by the fact that substituting conserved hydrophobic L131$^{34.51}$ to arginine abolished galanin activity (Fig. 6j). Intriguingly, residues at 34.54 or 34.55 are arginine or lysine in G_q-coupled GPCRs (Fig. 6h). These positively charged residues in ICL2 polarly interact with residues in αN of the $G\alpha_q$ subunit and probably be involved in the G_q-coupling of GPCRs (Fig. 6d–f). Together, these findings provide insight into the mechanism of galanin receptor-G protein engagement and expand our knowledge of the diverse roles of ICL2 in G protein coupling.

Importance of ICL2 of GAL2R in G_q protein-coupling selectivity. The above data suggest that ICL2 may serve as a

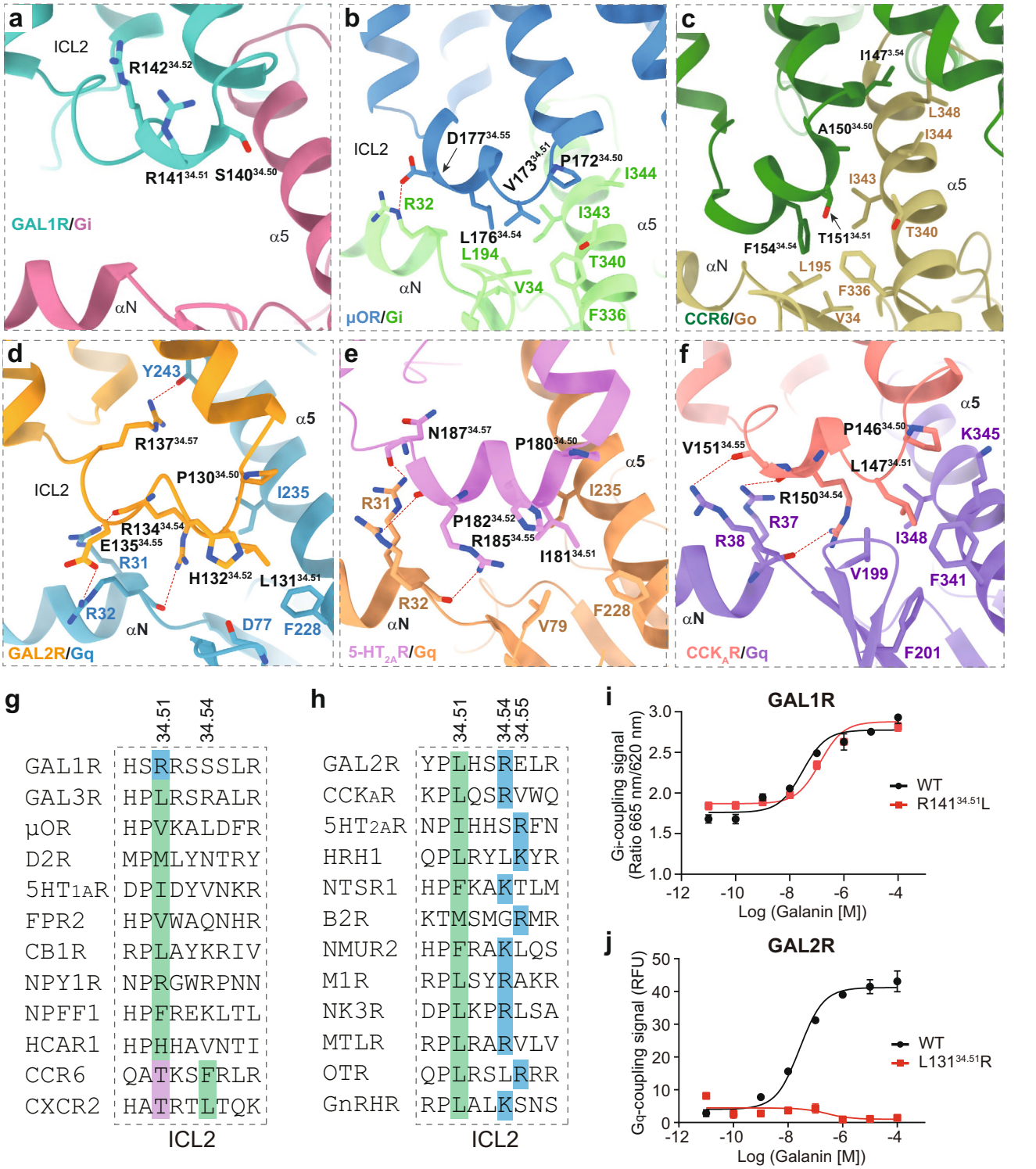

Fig. 6 Characteristics of ICL2 in G protein coupling of GAL1R and GAL2R. Detailed interaction between ICL2 of GAL1R (**a**), μOR (**b**), and CCR6 (**c**) and the $G\alpha_i$ subunit. Detailed interaction between ICL2 of GAL2R (**d**), 5-HT_{2A}R (**e**), and CCK_AR (**f**) and the $G\alpha_q$ subunit. **g** Sequence alignment of ICL2 of GAL1R and other class A GPCRs primarily coupled to G_i heterotrimer. The positive-charged arginine in ICL2 of GAL1R (blue) and polar residue threonine in ICL2 of CCR6 and CXCR2 (purple) at 34.51 are highlighted. Hydrophobic residues at 34.54 in CCR6 and CXCR2, which substantially contribute to the receptor-G_i coupling, are indicated in green. The conserved hydrophobic residues in other listed class A GPCRs at 34.51 are highlighted in green. **h** Sequence alignment of ICL2 of GAL1R and other class A GPCRs primarily coupled to G_q heterotrimer. The conserved hydrophobic residues at 34.51 are highlighted in green. The positively charged residues at 34.54 and 34.55 are indicated in blue. The swapping effects of $R141^{34.51}$ of GAL1R (**i**) and $L131^{34.51}$ of GAL2R (**j**) on G protein-coupling activity. Data shown are mean ± S.E.M. of three ($n = 3$, **i**) or four ($n = 4$, **j**) independent experiments. Source data are provided as a Source Data file.

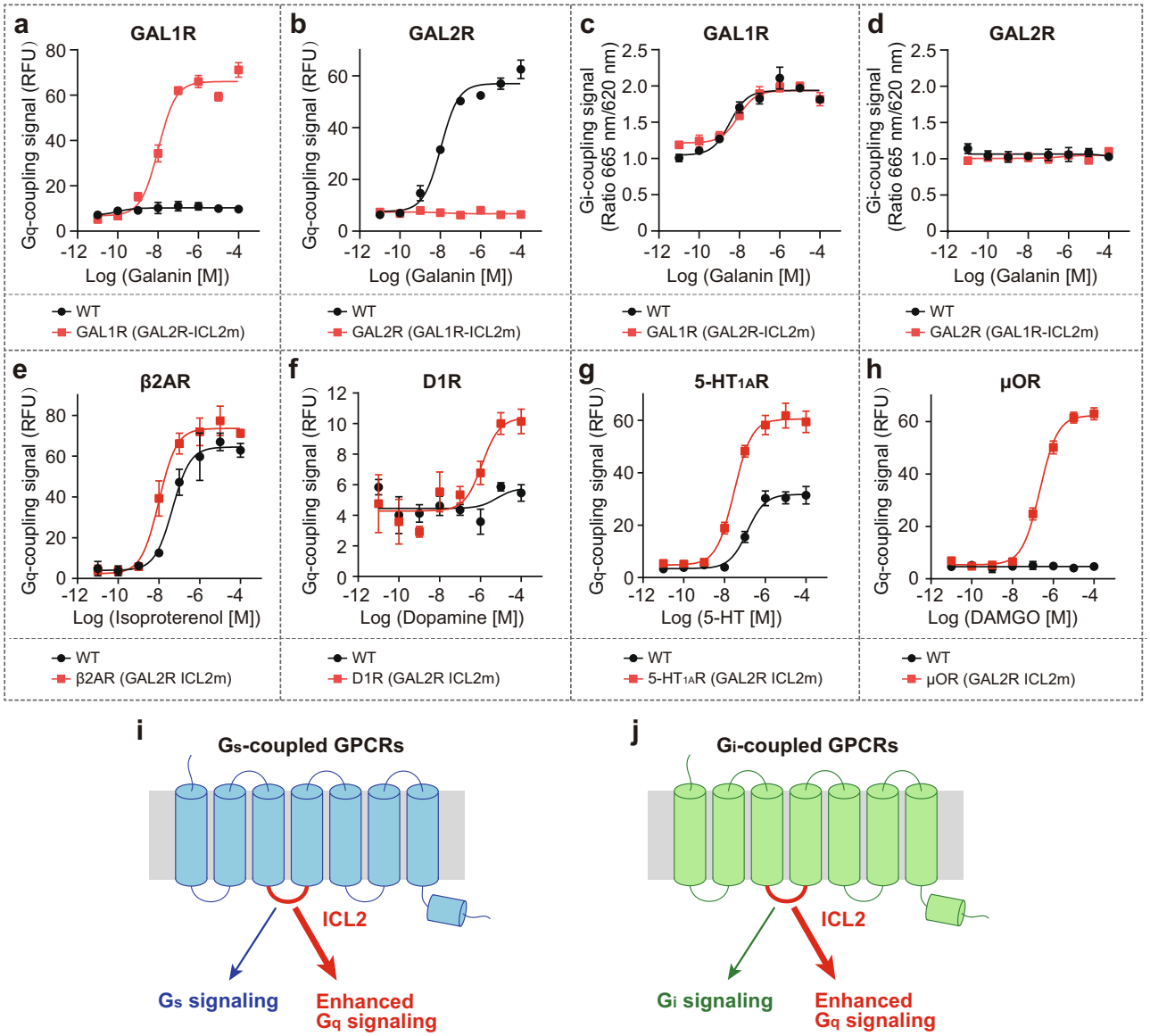

Fig. 7 Role of ICL2 of GAL2R in G_q-coupling selectivity. a, **b** The effects of ICL2 swapping between GAL1R (139-144) and GAL2R (129-135) on G_q-mediated signaling (calcium signal). GAL1R (GAL2R-ICL2m) represents mutated GAL1R containing the ICL2 from GAL2R. **c**, **d** The effects of ICL2 swapping between GAL1R (139-144) and GAL2R (129-135) on G_i-mediated signaling (cAMP signal). The effects of GAL2R ICL2 (129-135) substitution of G_s-coupled β2AR (137-142, **e**) and D1R (127-132, **f**) on G_q-mediated signaling. The effects of GAL2R ICL2 (129-135) substitution of G_i-coupled 5-HT_{1A}R (140-145, **g**) and μOR (173-178, **h**) on G_q-mediated signaling. Models to demonstrate roles of ICL2 on enhanced G_q-coupling activity of G_s- (**i**) and G_i-coupled class A GPCRs (**j**). Data shown are mean ± S.E.M. of three independent experiments ($n = 3$). Source data are provided as a Source Data file.

determinant of G_q protein selectivity for GAL2R. To prove this hypothesis, we further performed ICL2 swapping analysis and evaluated G_i- and G_q-coupling activities of chimeric galanin receptors. Consistent with our hypothesis, replacing ICL2 of GAL1R (139-144) with the cognate segment of GAL2R (129-135) enables GAL1R chimera elicits G_q-mediated signaling to a comparable extent of wild-type GAL2R (Fig. 7a). Conversely, the ICL2-swapped GAL2R abolished the G_q-coupling activity compared with the wild-type receptor (Fig. 7b). However, ICL2 swapping between GAL1R and GAL2R did not affect the G_i-coupling activity of the two receptors (Fig. 7c, d). These findings support the contention that ICL2 of GAL2R is closely involved in the GAL2R-G_q interaction.

Further investigation was directed toward exploring the commonality of ICL2 on G_q-coupling preference. Representative receptors coupling to G_s (β_2AR and D1R) and G_i proteins (5-HT_{1A}R and μOR) were applied for ICL2 substitution analysis (Fig. 7e–h). For predominantly G_s-coupled GPCRs, β_2AR showed moderate G_q-coupling activity, while D1R could not engage with G_q protein under our experimental condition. Compared with the WT receptor, the β_2AR chimera, with a replaced GAL2R ICL2, showed a 4.6-fold increased G_q-coupling activity (Fig. 7e). Interestingly, the ICL2 replacement enabled D1R chimera to engage G_q protein (Fig. 7f). Similar effects were observed in G_i-coupled 5-HT_{1A}R and μOR. GAL2R ICL2-replaced 5-HT_{1A}R displayed a notably increased G_q-coupling activity relative to the WT receptor (Fig. 7g), while ICL2 substitution evoked robust G_q-signaling of μOR, which failed to activate G_q in WT form (Fig. 7h). These results demonstrate that ICL2 of GAL2R can enhance G_q-coupling activity, even for receptors do not couple to G_q natively (Fig. 7i, j). Together, our structural and functional analyses reveal that ICL2 of GAL2R is essential to G_q-coupling

activity of either GAL2R or other G_s- and G_i-coupled GPCRs. Considering the complex roles of ICL2 on G protein coupling efficiency and a scarcity of structural evidence to unveil the rationale of ICL2-G_q coupling, these findings broaden the scope of our understanding of the GPCR-G_q coupling mechanism.

Discussion

In this paper, we reported two cryo-EM structures of galanin-bound GAL1R and GAL2R in complex with G_i protein and G_q chimera, respectively. Combined with mutagenesis and functional analyses, these structures reveal a unique binding pose of galanin, which significantly differs from the previously predicted galanin-binding model[10], as well as other peptide ligands of GPCRs. Two extensive hydrophobic regions, including ECL2 and a cluster comprising of TM6, ECL3, and TM7, clamp the N-terminal α-helical of galanin with high hydrophobicity onto the extracellular face of both galanin receptors, positing Y^{9P} inserting into a shallow helical pocket. The unique binding mode of galanin diversifies the peptide recognition mechanism for peptide GPCRs. Furthermore, due to the specific binding pose, galanin locates far away from the helical core. Alternatively, the galanin agonism signal may allosterically propagate through positively charged residues.

The distal C-terminus of the Gα subunit is thought to be important for its recognition by GPCRs[30–32], and is widely believed to be the primary determinant of GPCR-G protein coupling selectivity. Besides, the Gα subunit core is proven to be equally or even more important to G protein-coupling of individual GPCRs[14]. Recently, an emerging body of evidence supports the importance of ICLs in GPCR-G protein coupling. For $G_{q/11}$ protein selectivity, ICL3 substantially contributes to the G_q protein-coupling promiscuity of CCK_AR by interacting with a hydrophobic patch comprising $Y^{S6.02}$, $F^{H5.06}$, and $A^{H5.09}$ of the $G\alpha_q$ subunit[33]. ICL2 of the receptor is involved in the secondary $G_{i/o}$ coupling[16]. In this study, structures of galanin receptor complexes show that the conserved hydrophobic residue at 34.51 is absent in ICL2 of GAL1R, which displays minor importance on GAL1R coupling to G_i protein even though substituting $R141^{34.51}$ with a hydrophobic leucine. Intriguingly, ICL2 of GAL2R was further identified to be critical to G_q-coupling. The importance of ICL2 on G_q-coupling activity can be extended to other G_s- and G_i-coupled class A GPCRs, making ICL2 a putative universal determinant for G_q-coupling selectivity. Together, our structures provide a framework for deepening understanding of the unique mechanism of peptide recognition and allosteric activation of galanin receptors, offering a new opportunity for designing galanin receptor-targeted drugs. Our findings also illustrate the basis of G protein-coupling of galanin receptors and clarify the commonality in the importance of ICL2 on G_q-coupling of GAL2R and other class A GPCRs.

Methods

Constructs. Human GAL1R (residues 1–349) was cloned with an N-terminal FLAG and C-terminal His8 tags. Human GAL2R (residues 1–333) was cloned with an N-terminal FLAG tag and C-terminal followed with LgBiT[18]. The native signal peptide was replaced with haemagglutinin (HA) to increase protein expression. Bovine $G\alpha_{i1}$ were incorporated with four dominant-negative mutations (S47N, G203A, E245A, and A326S) by site-directed mutagenesis to decrease the affinity of nucleotide-binding and increase the stability of the Gαβγ complex[34]. The $G\alpha_q$ was designed based on a mini$G\alpha_s$ skeleton with N-terminus replaced by G_{i1} for the binding of scFv16[35]. Rat Gβ1 was cloned with an N-terminal His6 tag. All the constructs, including bovine Gγ2 and scFv16, were cloned into a pFastBac vector using homologous recombination (CloneExpress One Step Cloning Kit, Vazyme), respectively.

Expression and purification of Nb35. Nanobody-35 (Nb35) with a C-terminal His6 tag, was expressed and purified as previously described[18]. Nb35 was purified by nickel affinity chromatography, followed by size-exclusion chromatography using a HiLoad 16/600 Superdex 75 column (Cytiva) and finally spin concentrated to 3 mg/mL.

Complexes expression and purification. For galanin-GAL1R-G_i complex, GAL1R, $G\alpha_i$, Gβ1, and Gγ2, as well as scFv16, were co-expressed in *sf*9 insect cells using the Bac-to-Bac baculovirus expression system. Cell pellets were thawed and lysed in 20 mM HEPES pH 7.4, 100 mM NaCl, 10% glycerol, 5 mM MgCl2, and 5 mM CaCl2 supplemented with Protease Inhibitor Cocktail, EDTA-Free (TargetMol). The galanin-GAL1R-G_i complex was formed in membranes by the addition of 5 μM galanin peptide (synthesized by GenScript) and 25 mU/mL apyrase. The suspension was incubated for 1 h at room temperature. The membrane was then solubilized using 0.5% (w/v) lauryl maltose neopentylglycol (LMNG, Anatrace), 0.1% (w/v) cholesteryl hemisuccinate TRIS salt (CHS, Anatrace) for 2 h at 4 °C. The supernatant was collected by centrifugation at 64,000 × *g* for 45 min and then incubated with Anti-DYKDDDDK Affinity Beads (SMART Lifesciences) for 2 h at 4 °C. The resin was then washed with 10 column volumes of 20 mM HEPES pH 7.4, 100 mM NaCl, 10% glycerol, 2 mM MgCl2, 2 mM CaCl2, 0.01% (w/v) LMNG, 0.002%(w/v) CHS, 1 μM galanin and further washed with 10 column volumes of same buffer plus 0.1%(w/v) digitonin, and finally eluted using 0.2 mg/mL Flag peptide. The complex was then concentrated using an Amicon Ultra Centrifugal Filter (MWCO 100 kDa) and injected onto a Superdex200 10/300 GL column (GE Healthcare) equilibrated in the buffer containing 20 mM HEPES pH 7.4, 100 mM NaCl, 2 mM MgCl2, 2 mM CaCl2, 0.05 (w/v) digitonin, and 1 μM galanin. The complex fractions were collected and concentrated for electron microscopy experiments. For the galanin-GAL2R-G_q complex, GAL2R, $G\alpha_q$, Gβ1, and Gγ2 were co-expressed in *sf*9 insect cells before purification. The purification procedure was similar to GAL1R except for the addition of Nb35 and no addition of digitonin, as well as the final size-column equilibrated with 0.00075% (w/v) LMNG, 0.00025% (w/v) GDN and 0.0002% (w/v) CHS instead of 0.05 (w/v) digitonin.

Cryo-EM grid preparation and data collection. Three microliters of the purified galanin-GAL1R-G_i-scFv16 and galanin-GAL2R-G_q-Nb35 complexes at the concentration of about 26 mg/mL and 28 mg/mL, respectively, were applied onto glow-discharged holey carbon grids (Quantifoil R1.2/1.3). Excess samples were blotted for 4 s with a blot force of 10 and were vitrified by plunging into liquid ethane using a Vitrobot Mark IV (Thermo Fisher Scientific). Frozen grids were transferred to liquid nitrogen and stored for data acquisition. Cryo-EM imaging was performed on a Titan Krios at 300 kV in the Center of Cryo-Electron Microscopy, Zhejiang University (Hangzhou, China). Micrographs were recorded using a Gatan K2 Summit detector in counting mode with a pixel size of 1.014 Å using the SerialEM software[36]. Movies were obtained at a dose rate of about 8.0 electrons per $Å^2$ per second with a defocus ranging from −0.5 to −2.5 μm. The total exposure time was 8 s, and 40 frames were recorded per micrograph. A total of 2571 and 2861 movies were collected for galanin-GAL1R-G_i-scFv16 and galanin-GAL2R-G_q-Nb35 complexes, respectively.

Cryo-EM data processing. Cryo-EM image stacks were aligned using MotionCor2.1[37] and Contrast transfer function (CTF) parameters for each micrograph were estimated by Gctf[38]. The following data processing was performed using RELION-3.0-beta2[39].

For the galanin-GAL1R-G_i-scFv16 complex, automated particle selection yielded 2,036,106 particle projections. The projections were subjected to reference-free 2D classification to discard poorly defined particles, producing 2,001,019 particle projections for further processing. This subset of particle projections was subjected to a round of maximum-likelihood-based three-dimensional classification with a pixel size of 2.028 Å. A selected subset containing 797,234 projections was used to obtain the final map using a pixel size of 1.014 Å. Further 3D classification focusing the alignment on the receptor produced one good subset accounting for 492,139 particles, which were subsequently subjected to 3D refinement, CTF refinement, and Bayesian polishing. After another round of 3D classification focusing on the part of the receptor close to the extracellular domain, final refinement generated a map with an indicated global resolution of 2.7 Å at an FSC of 0.143.

For the galanin-GAL2R-G_q-Nb35 complex, 1,835,716 particle projections from the automated particle picking were subjected to 2D classification, producing 732,428 particle projections for further processing. This subset of particle projections was subjected to a round of maximum-likelihood-based three-dimensional classification with a pixel size of 2.028 Å. A selected subset containing 480,664 projections was used to obtain the final map using a pixel size of 1.014 Å. Further 3D classification focusing the alignment on the complex produced one good subset accounting for 255,766 particles, which were subsequently subjected to 3D refinement and Bayesian polishing. The final refinement generated a map with an indicated global resolution of 2.6 Å.

Model building and refinement. The initial templates of GAL1R and GAL2R were derived from a homology-based predicted model downloaded in the GPCRdb[40]. Models of G_i and G_q heterotrimers were adopted from the 5-HT-5-HT_{1D}-G_i complex (PDB: 7E32) and the 25-CN-NBOH-bound G_q-coupled 5-HT_{2A}

Serotonin Receptor (PDB: 6WHA), respectively. The coordinate of the LA-PTH-PTH1R-G_s complex (PDB: 6NBF) was used to generate the initial model of Nb35. Models were docked into the EM density map using UCSF Chimera[41]. The initial models were then subjected to iterative rounds of manual adjustment based on the side-chain densities of bulky aromatic amino acids in Coot[42] and automated refinement in Rosetta[43] and PHENIX[44]. The final refinement statistics were validated using the module "comprehensive validation (cryo-EM)" in PHENIX[45]. The final refinement statistics are provided in Supplementary Table 1.

Ligand-binding assays. Ligand binding was performed with a homogeneous time-resolved fluorescence-based assay. N-terminal-SNAP-tagged GAL1R or GAL2R and full-length galanin labeled with the dye A2 on an additional cysteine at the C-terminal end of the peptide (galanin-A2, synthesized by Vazyme, China) were used as previously described[46].

HEK293 cells transfected with SNAP-GAL1R or SNAP-GAL2R (WT or mutants) were seeded at a density of 1×10^6 cells into 3 cm dish and incubated for 24 h at 37 °C in 5% CO_2. Cell culture medium was removed and Tag-lite labeling medium with 100 nM of SNAP-Lumi4-Tb (Cisbio, SSNPTBC) was added, and the cells were further incubated for 1 h at 37 °C in 5% CO_2. The excess of SNAP-Lumi4-Tb was then removed by washing 4 times with 1 ml of Tag-lite labeling medium.

For saturation binding experiments, we incubated cells with increasing concentrations of galanin-A2 in the presence or absence of 100 μM unlabeled galanin for 1 h at room temperature (R.T.). For competition experiments, cells were incubated with 50 nM galanin-A2 in the presence of increasing concentrations of ligands to be tested for 1 h at R.T. Signal was detected using the Multimode Plate Reader (PerkinElmer EnVision) equipped with an HTRF optic module allowing a donor excitation at 340 nm and a signal collection both at 665 nm and at 620 nm. HTRF ratios were obtained by dividing the acceptor signal (665 nm) by the donor signal (620 nm). Saturation binding experiments and competition experiments were analyzed by binding-saturation and dose–response curve using GraphPad Prism 8.0 (GraphPad Software) respectively. K_d, B_{max} and IC_{50} values were calculated using nonlinear regression (curve fit). After fitting the competition binding curves, the inhibition constant (K_i) of the unlabeled ligands was calculated by using the Cheng–Prusoff equation:

$$Ki = \frac{IC_{50}}{1 + \frac{[L]}{K_d}} \quad (1)$$

where [L] is the concentration of fluorescent ligand in nM and the dissociation constant (K_d) is the K_d of fluorescent ligand in nM. Data are means ± S.E.M. from at least three independent experiments performed in technical triplicates.

Calcium assay. To assess the function of galanin mutants on WT galanin receptors, or the function of galanin on receptor mutants (mutations in the binding pocket and activation cascade), calcium assays were performed in HEK293/$G\alpha_{16}$[47,48] cells transfected with WT or mutant galanin receptors. To assess the function of ICL2 on $G\alpha_q$ coupling, calcium assay were performed in HEK293 cells transfected with various receptors. Briefly, cells transfected with WT or mutant receptors were seeded at a density of 4×10^4 cells per well into 96-well culture plates and incubated for 24 h at 37 °C in 5% CO_2.The cells were then incubated with 2 μmol/L Fluo-4 AM in HBSS (5.4 mmol/L KCl, 0.3 mmol/L Na_2HPO_4, 0.4 mmol/L KH_2PO_4, 4.2 mmol/L $NaHCO_3$, 1.3 mmol/L $CaCl_2$, 0.5 mmol/L $MgCl_2$, 0.6 mmol/L $MgSO_4$, 137 mmol/L NaCl, 5.6 mmol/L D-glucose and 250 μmol/L sulfinpyrazone, pH 7.4) at 37 °C for 40 min. After thorough washing, 50 μL of HBSS was added. After incubation at R.T. for 10 min, 25 μL of agonist was dispensed into the well using a FlexStation III microplate reader (Molecular Devices), and the intracellular calcium change was recorded at an excitation wavelength of 485 nm and an emission wavelength of 525 nm. EC_{50} and E_{max} values for each curve were calculated by GraphPad Prism 8.0. Data are means ± S.E.M. from at least three independent experiments performed in technical triplicates.

cAMP assay. The cAMP assays were performed in HEK293 cells transfected with WT or mutant receptors. Briefly, cells were harvested and re-suspended in PBS containing 500 μM IBMX at a density of 2×10^5 cells/mL. Cells were then plated onto 384-well assay plates at 1000 cells/5 μL/well. Another 5 μL PBS containing different concentrations of galanin with 2 μM forskolin were added to the cells and the incubation lasted for 30 min at 37 °C. Intracellular cAMP levels were tested by the LANCE Ultra cAMP kit (PerkinElmer, TRF0264) and the Multimode Plate Reader (PerkinElmer Envision) according to the manufacturer's instructions. Data were analyzed using the dose–response curve in GraphPad Prism 8.0. Data are means ± S.E.M. from at least three independent experiments performed in technical triplicates.

Data analysis. All functional study data were analyzed using Prism 8 (GraphPad) and presented as means ± S.E.M. from at least three independent experiments. Concentration-response curves were evaluated with a three-parameter logistic equation. EC_{50} is calculated with the Sigmoid three-parameter equation. The significance was determined with two-side, one-way ANOVA with Tukey's test, and $^*P < 0.01$; $^{**}P < 0.001$, and $^{***}P < 0.0001$ *vs.* wild-type (WT) was considered statistically significant.

Reporting summary. Further information on research design is available in the Nature Research Reporting Summary linked to this article.

Data availability

The atomic coordinates and the electron microscopy maps have been deposited in the Protein Data Bank (PDB) under accession number 7WQ3 (Fo-wing), 7WQ4 (Fo-wing) and Electron Microscopy Data Bank (EMDB) accession number EMD-32698 (Fo-wing) and EMD-32699 (Fo-wing) for the galanin-GAL1R-G_i-ScFv16 and the galanin-GAL2R-G_q-Nb35 complex, respectively. Source data are provided with this paper.

Received: 15 October 2021; Accepted: 24 February 2022;
Published online: 15 March 2022

References

1. Sahbaz, B. D. & Iyison, N. B. *Neuropeptides as Ligands for GPCRs*. (IntechOpen, London, 2018).
2. Tikhonova, I. G., Gigoux, V. & Fourmy, D. Understanding Peptide Binding in Class A G Protein-Coupled Receptors. *Mol. Pharm.* **96**, 550–561 (2019).
3. Lang, R. et al. Physiology, signaling, and pharmacology of galanin peptides and receptors: three decades of emerging diversity. *Pharm. Rev.* **67**, 118–175 (2015).
4. Liu, Z., Xu, Y., Wu, L. & Zhang, S. Evolution of galanin receptor genes: insights from the deuterostome genomes. *J. Biomol. Struct. Dyn.* **28**, 97–106 (2010).
5. Land, T. et al. Linear and cyclic N-terminal galanin fragments and analogs as ligands at the hypothalamic galanin receptor. *Int J. Pept. Protein Res.* **38**, 267–272 (1991).
6. Wang, S., He, C., Hashemi, T. & Bayne, M. Cloning and expressional characterization of a novel galanin receptor. Identification of different pharmacophores within galanin for the three galanin receptor subtypes. *J. Biol. Chem.* **272**, 31949–31952 (1997).
7. Landry, M., Roche, D., Vila-Porcile, E. & Calas, A. Effects of centrally administered galanin (1-16) on galanin expression in the rat hypothalamus. *Peptides* **21**, 1725–1733 (2000).
8. Liu, H. X. et al. Receptor subtype-specific pronociceptive and analgesic actions of galanin in the spinal cord: selective actions via GalR1 and GalR2 receptors. *Proc. Natl Acad. Sci. USA* **98**, 9960–9964 (2001).
9. Berthold, M. et al. Mutagenesis and ligand modification studies on galanin binding to its GTP-binding-protein-coupled receptor GalR1. *Eur. J. Biochem.* **249**, 601–606 (1997).
10. Church, W. B., Jones, K. A., Kuiper, D. A., Shine, J. & Iismaa, T. P. Molecular modelling and site-directed mutagenesis of human GALR1 galanin receptor defines determinants of receptor subtype specificity. *Protein Eng.* **15**, 313–323 (2002).
11. Lundstrom, L., Sollenberg, U. E., Bartfai, T. & Langel, U. Molecular characterization of the ligand binding site of the human galanin receptor type 2, identifying subtype selective interactions. *J. Neurochem.* **103**, 1774–1784 (2007).
12. Jurkowski, W., Yazdi, S. & Elofsson, A. Ligand binding properties of human galanin receptors. *Mol. Membr. Biol.* **30**, 206–216 (2013).
13. Flock, T. et al. Selectivity determinants of GPCR-G-protein binding. *Nature* **545**, 317–322 (2017).
14. Okashah, N. et al. Variable G protein determinants of GPCR coupling selectivity. *Proc. Natl Acad. Sci. USA* **116**, 12054–12059 (2019).
15. Sandhu, M. et al. Conformational plasticity of the intracellular cavity of GPCR-G-protein complexes leads to G-protein promiscuity and selectivity. *Proc. Natl Acad. Sci. USA* **116**, 11956–11965 (2019).
16. Kim, H. R. et al. Structural mechanism underlying primary and secondary coupling between GPCRs and the Gi/o family. *Nat. Commun.* **11**, 3160 (2020).
17. Maeda, S. et al. Development of an antibody fragment that stabilizes GPCR/G-protein complexes. *Nat. Commun.* **9**, 3712 (2018).
18. Duan, J. et al. Cryo-EM structure of an activated VIP1 receptor-G protein complex revealed by a NanoBiT tethering strategy. *Nat. Commun.* **11**, 4121 (2020).
19. Koehl, A. et al. Structure of the micro-opioid receptor-Gi protein complex. *Nature* **558**, 547–552 (2018).
20. Yin, Y. L. et al. Molecular basis for kinin selectivity and activation of the human bradykinin receptors. *Nat. Struct. Mol. Biol.* **28**, 755–761 (2021).
21. Wang, Y. et al. Molecular recognition of an acyl-peptide hormone and activation of ghrelin receptor. *Nat. Commun.* **12**, 5064 (2021).

22. Wennerberg, A. B., Cooke, R. M., Carlquist, M., Rigler, R. & Campbell, I. D. A 1H NMR study of the solution conformation of the neuropeptide galanin. *Biochem Biophys. Res. Commun.* **166**, 1102–1109 (1990).
23. Morris, M. B. et al. Structural and biochemical studies of human galanin: NMR evidence for nascent helical structures in aqueous solution. *Biochemistry* **34**, 4538–4545 (1995).
24. Ohman, A. et al. NMR study of the conformation and localization of porcine galanin in SDS micelles. Comparison with an inactive analog and a galanin receptor antagonist. *Biochemistry* **37**, 9169–9178 (1998).
25. Ohtaki, T. et al. Isolation and cDNA cloning of a novel galanin-like peptide (GALP) from porcine hypothalamus. *J. Biol. Chem.* **274**, 37041–37045 (1999).
26. Berger, A. et al. Galanin receptor subtype GalR2 mediates apoptosis in SH-SY5Y neuroblastoma cells. *Endocrinology* **145**, 500–507 (2004).
27. Kim, D. K. et al. Coevolution of the spexin/galanin/kisspeptin family: Spexin activates galanin receptor type II and III. *Endocrinology* **155**, 1864–1873 (2014).
28. Zhou, Q. et al. Common activation mechanism of class A GPCRs. *Elife* **8**, e50279 (2019).
29. Wasilko, D. J. et al. Structural basis for chemokine receptor CCR6 activation by the endogenous protein ligand CCL20. *Nat. Commun.* **11**, 3031 (2020).
30. Conklin, B. R., Farfel, Z., Lustig, K. D., Julius, D. & Bourne, H. R. Substitution of three amino acids switches receptor specificity of Gq alpha to that of Gi alpha. *Nature* **363**, 274–276 (1993).
31. Conklin, B. R. et al. Carboxyl-terminal mutations of Gq alpha and Gs alpha that alter the fidelity of receptor activation. *Mol. Pharm.* **50**, 885–890 (1996).
32. Kostenis, E., Gomeza, J., Lerche, C. & Wess, J. Genetic analysis of receptor-Galphaq coupling selectivity. *J. Biol. Chem.* **272**, 23675–23681 (1997).
33. Liu, Q. et al. Ligand recognition and G-protein coupling selectivity of cholecystokinin A receptor. *Nat. Chem. Biol.* **17**, 1238–1244 (2021).
34. Xu, P. et al. Structural insights into the lipid and ligand regulation of serotonin receptors. *Nature* **592**, 469–473 (2021).
35. Yin, Y. L. et al. Molecular basis for kinin selectivity and activation of the human bradykinin receptors. *Nat. Struct. Mol. Biol.* **28**, 755–761 (2021).
36. Mastronarde, D. N. Automated electron microscope tomography using robust prediction of specimen movements. *J. Struct. Biol.* **152**, 36–51 (2005).
37. Zheng, S. Q. et al. MotionCor2: anisotropic correction of beam-induced motion for improved cryo-electron microscopy. *Nat. Methods* **14**, 331–332 (2017).
38. Zhang, K. Gctf: Real-time CTF determination and correction. *J. Struct. Biol.* **193**, 1–12 (2016).
39. Scheres, S. H. RELION: implementation of a Bayesian approach to cryo-EM structure determination. *J. Struct. Biol.* **180**, 519–530 (2012).
40. Kooistra, A. J. et al. GPCRdb in 2021: integrating GPCR sequence, structure and function. *Nucleic Acids Res.* **49**, D335–D343 (2021).
41. Pettersen, E. F. et al. UCSF Chimera–a visualization system for exploratory research and analysis. *J. Comput. Chem.* **25**, 1605–1612 (2004).
42. Emsley, P. & Cowtan, K. Coot: model-building tools for molecular graphics. *Acta Crystallogr D. Biol. Crystallogr* **60**, 2126–2132 (2004).
43. Wang, R. Y. et al. Automated structure refinement of macromolecular assemblies from cryo-EM maps using Rosetta. *Elife* **5**, (2016).
44. Adams, P. D. et al. PHENIX: a comprehensive Python-based system for macromolecular structure solution. *Acta Crystallogr D. Biol. Crystallogr* **66**, 213–221 (2010).
45. Afonine, P. V. et al. New tools for the analysis and validation of cryo-EM maps and atomic models. *Acta Crystallogr D. Struct. Biol.* **74**, 814–840 (2018).
46. Leyris, J. P. et al. Homogeneous time-resolved fluorescence-based assay to screen for ligands targeting the growth hormone secretagogue receptor type 1a. *Anal. Biochem* **408**, 253–262 (2011).
47. Coward, P., Chan, S. D., Wada, H. G., Humphries, G. M. & Conklin, B. R. Chimeric G proteins allow a high-throughput signaling assay of Gi-coupled receptors. *Anal. Biochem* **270**, 242–248 (1999).
48. Zhu, T., Fang, L. Y. & Xie, X. Development of a universal high-throughput calcium assay for G-protein- coupled receptors with promiscuous G-protein Galpha15/16. *Acta Pharm. Sin.* **29**, 507–516 (2008).
49. Durrant, J. D., Votapka, L., Sorensen, J. & Amaro, R. E. POVME 2.0: An Enhanced Tool for Determining Pocket Shape and Volume Characteristics. *J. Chem. Theory Comput* **10**, 5047–5056 (2014).

Acknowledgements

The cryo-EM data were collected at the Center of Cryo-Electron Microscopy, Zhejiang University. We thank the staff of the Center of Cryo-Electron Microscopy, Zhejiang University for instrument support. This work was partially supported by National Natural Science Foundation (32171187 to Y.J., 82121005 to X.X., Y.J., and H.E.X., 81730099 to X.X., 81922071 to Y.Z., 32130022 to H.E.X.), the Ministry of Science and Technology (China) grants (2018YFA0507002 to H.E.X. and 2019YFA0508800 to Y.Z.), the Shanghai Municipal Science and Technology Major Project (2019SHZDZX02 to H.E.X.), Shanghai Municipal Science and Technology Major Project (H.E.X.); the CAS Strategic Priority Research Program (XDB37030103 to H.E.X.), and the Shanghai Municipal Science and Technology Commission Grant (20S11903200 to X.X.), the Zhejiang Province Science Fund for Distinguished Young Scholars (LR19H310001 to Y.Z.); the MOE Frontier Science Center for Brain Science & Brain-Machine Integration, Zhejiang University (to Y.Z.); the Science and Technology Commission of Shanghai Municipal (20431900100 to H.J.); the Jack Ma Foundation (2020-CMKYGG-05 to H.J.); and Shanghai Sailing Program (19YF1457600 to Q.L.); and The Youth Innovation Promotion Association of Chinese Academy of Science (2018319 to X.C).

Author contributions

J.D. designed the expression constructs, purified the galanin receptor complexes, prepared the final samples for negative stain and data collection toward the structures, participated in figure and manuscript preparation; D.S. performed specimen screening by negative-stain EM, cryo-EM grid preparation, cryo-EM data collection, map calculations, and model building, supervised by Y.Z.; S.G. and T.Z. designed all of the mutants for the ligand-binding pockets and executed all the cellular experiments including the ligand-binding assay, calcium assay, and cAMP accumulation assay supervised by X.X.; X.H. performed the binding pocket calculation, supervised by X.C. and H.J.; W.Y. designed the G_q protein construct; P.X., Y.-J.J., L.C., J.L., H.Z., Q.L., and Y.S. participated in the experiments; J.D., S.G., and Y.J. analyzed the structures, prepared the figures, and wrote the manuscript; Y.J., H.E.X. conceived the project, initiated collaborations with X.X. and Y.Z.; Y.J., H.E.X., X.X., and Y.Z. wrote the manuscript with input from all authors.

Competing interests

The authors declare no competing interests.

Additional information

Supplementary information The online version contains supplementary material available at https://doi.org/10.1038/s41467-022-29072-3.

Correspondence and requests for materials should be addressed to H. Eric Xu, Yan Zhang, Xin Xie or Yi Jiang.

Peer review information *Nature Communications* thanks Alisa Glukhova, Hugo Gutierrez-de-Teran and the other, anonymous, reviewer(s) for their contribution to the peer review of this work.

Reprints and permission information is available at http://www.nature.com/reprints

Publisher's note Springer Nature remains neutral with regard to jurisdictional claims in published maps and institutional affiliations.